Simple and robust architecture of a laser system for atom interferometry

Sumit Sarkar, Raphaël Piccon, Sébastien Merlet, Franck Pereira dos Santos

Research Article | Vol. 30, No. 3 / 31 Jan 2022 / Optics Express 3358
Optics EXPRESS

Simple and robust architecture of a laser system for atom interferometry

SUMIT SARKAR, RAPHAËL PICCON, SÉBASTIEN MERLET, AND FRANCK PEREIRA DOS SANTOS*

LNE-SYRTE, Observatoire de Paris, Université PSL, CNRS, Sorbonne Université, 61 Avenue de l'Observatoire, 75014 Paris, France
franck.pereira@obspm.fr

Abstract: We report a compact and robust architecture of a versatile laser system that allows the implementation of several advanced atom interferometry techniques, such as Bragg diffraction, Bloch oscillations, or single and double Raman diffraction. A low noise, frequency tunable fiber-laser ($\lambda = \sim$1560 nm) serves as the seed. A couple of fiber-coupled amplifiers followed by two fibered second-harmonic generators produce a pair of phase-locked, frequency-controllable laser beams at 780 nm. Manipulating frequencies of individual laser beams at $\lambda = 1560$ nm before the amplifiers, facilitates achieving a maximum relative detuning of ± 20 MHz, while maintaining a constant output power. We present the scheme to implement Raman spectroscopy using our laser system and discuss its advantages. Finally, the overall performance of the laser setup has been evaluated by realizing interferometers in copropagating Ramsey-Raman and counterpropagating Bragg configuration.

1. Introduction

Atom interferometry (AI) is one of the promising technologies in the field of quantum metrology and quantum sensing [1]. AI-based sensors have already been employed to measure absolute gravity [2–6], gravity gradient [7–9], rotation [10,11], Newtonian gravitational constant [12,13], etc. However, in most of the cases, such systems, realized in laboratories are relatively bulky in comparison to their commercial analogues [14]. Therefore, the construction of a more compact yet simple and robust system remains a challenging problem in this research area. Further, the application of novel techniques like Large Momentum Transfer (LMT) beam-splitters [15], requires adoption of appreciable complexity in the laser system. In practice, the laser system should allow manipulating a range of parameters (such as pulse intensity, pulse shaping, laser frequency, etc.) to study the trade-off between the amount of coupling and spontaneous emission. There have been several appreciable efforts in constructing simplified laser systems to adopt specific requirements for implementing novel techniques and addressing different problems of interest. Laser systems offering extremely low phase noise [16], high powers ranging up to few tens of Watts [17–19], compact and portable design [20–30], and frequency shift using serrodyne modulation [31] have already been reported.

In this article, we present our laser architecture built for realizing a gradiometer in Raman or Bragg geometry. The laser system uses a single 1560 nm laser input and employs frequency doubling techniques to produce two phase-locked outputs at 780 nm. The setup is based on fiber-coupled geometry [20,32] and hence offers better efficiency, stability, and robustness in comparison to a free space geometry. The two outputs of the laser system can be relatively detuned by $\sim \pm$ 20 MHz without sacrificing the output power in each of them. We describe the schemes used in our system to realize velocity selection and double diffraction [33] using Raman spectroscopy. We also characterize the residual phase noise of the laser system with an FFT analyzer and hence estimate a contribution of about 2.6 mrad/shot (1 cycle ≈ 1 s) to the sensitivity of a Mach-Zehnder interferometer with $2T_{MZ} = 240$ ms (where, the total duration of

#447073 https://doi.org/10.1364/OE.447073
Journal © 2022 Received 27 Oct 2021; revised 19 Dec 2021; accepted 3 Jan 2022; published 18 Jan 2022

Optics EXPRESS

the Mach-Zehnder interferometer = $2T_{MZ}$). We further demonstrate experimentally the efficiency of the phase lock by realizing a copropagating Ramsey interferometer with ^{87}Rb atoms. Finally, we present the results of the demonstration of a Bragg interferometer using our laser system.

2. Design

The architecture of the laser schematic can be broadly divided into three parts. The main part is shown in Fig. 1(a). We use a narrow linewidth, single-frequency Erbium-doped fiber-laser (Koheras Basik E15) from NKT Photonics as a seed to the system. The laser operates around 1560 nm and allows tunability of ~ ± 500 pm around the center wavelength. The maximum output of this laser is 40 mW with power stability of the order of 0.03 dB. The output of the laser is split into two paths in a 9:1 ratio using a fiber-coupled beam splitter (FBS). The smaller part is used to monitor the wavelength of the laser. The larger part of the output is fed to an Erbium fiber-amplifier (labeled as 'PAMP' in Fig. 1(a), Model: Keopsys, CEFA-C-BO-HP) capable of producing 25 dBm output. This pre-amplifier is operated at 20 dBm and the output of this pre-amplifier is separated into two arms again using an FBS. Each of these arms (labeled as 'Arm 1' and 'Arm 2' in Fig. 1(a)) consists of identical fiber-based optical components to produce a pair of optical laser beams for the implementation of Raman or Bragg geometry. The basic structure of each arm is made of a fiber-coupled acousto-optic modulator (AOM), followed by a fibered amplifier and a fiber-coupled second harmonic generator (SHG). The two AOMs ('AOM 1' and 'AOM 2') are driven by the outputs of a pair of synchronized Direct Digital Synthesizer (DDS). This allows producing a pair of relatively detuned optical beams to meet the appropriate Bragg or Bloch conditions. The outputs of these AOMs are fed to a couple of amplifiers (labeled as 'AMP 1' and 'AMP 2' in Fig. 1(a), Model: Keopsys, CEFA-C-BO-HP) operated at 30 dBm output power in the standard automatic power control (APC) mode. The output of the two amplifiers are then made to go through fibered periodically poled lithium niobate (PPLN) waveguide modules (NTT Electronics: WH-0780-000-A-B-C) [34] for the purpose of frequency doubling (shown by 'SHG 1' and 'SHG 2' in Fig. 1(a)). All the optical elements in between the seed laser and the output of the AOMs are mounted in a 19" 2U rack, while the pair of Amplifiers and frequency doublers are installed on the free space breadboard where they occupy a volume of 25 cm × 22 cm × 12 cm.

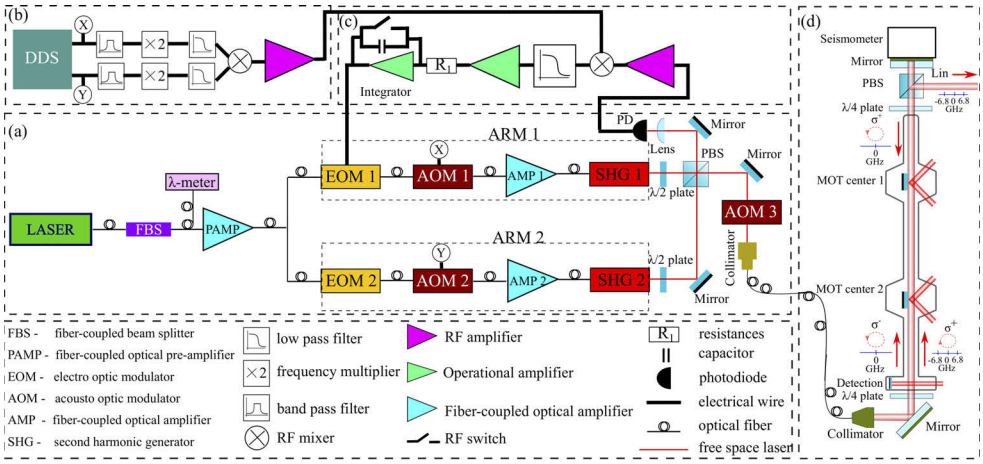

Fig. 1. (a) Basic architechture of the laser system; (b) Preparation of the reference signal for the differential phase-lock; (c) Implementation of the differential phase lock; (d) experimental setup to realize an atom gradiometer.

Optics EXPRESS

Unlike a few similar preceding designs mentioned earlier, the AOMs used to control the relative frequency offset between the optical outputs are placed before the amplifiers and SHGs and they are operated in single-diffraction geometry. The amplifiers produce constant optical output power until the input optical power is less than 8 dBm. This allows changing the operating frequencies of the AOMs by ±5 MHz while the optical output of the pre-amplifier is set to 20 dBm. Hence, we achieve two optical beams after the SHGs with a maximum final frequency difference of ± 20 MHz, which is sufficient to drive the Bragg or Bloch transitions in our setup. The outputs of the two SHGs propagate in free space and are mixed into a polarizing beam splitter (PBS). Among the two outputs of this PBS, the weaker one is made to fall on a fast photodiode (labeled as 'PD' in Fig. 1(a)) to track the phase difference in the two paths and utilize this signal to lock the differential phase. The stronger output contains two orthogonally polarized relatively detuned pairs of optical beams. These overlapping laser beams then pass through an AOM (labeled as 'AOM 3' in Fig. 1(a)) operating in a fixed-frequency single-pass configuration. However, by varying the RF amplitude into the AOM, the desired pulse shape for the implementation of the Bloch/Bragg/Raman process is achieved. The output of this AOM is injected into an optical fiber with a large mode area which delivers the light to the sensor head of the interferometer setup.

In addition to the optical components mentioned earlier, each arm contains an electro-optic phase modulator (EOM, Model: MPZ-LN-10 from iXBlue Photonics) after the pre-amplifier. Each EOM (labeled as 'EOM 1' and 'EOM 2' in Fig. 1(a)) has a different role to play in the setup. We use 'EOM 2' for generating frequency sidebands to produce Raman beams [21] for the experiment. Such an optical sideband is used in conjugation with the optical beam of the other arm to realize a Raman geometry for ^{87}Rb atoms. A more detailed description of the implementation of the Raman spectroscopy and interferometer is provided in section 3. We use most of the main optical elements in the fiber-coupled configuration. The advantage of such a choice is to avoid losses, misalignment, distortion of wavefronts and maintain the quality factor (M^2) of the optical beam. However, there is a disadvantage to the free space configuration. Since light travels several meters through these optical fibers and especially in the fibered amplifiers, the two optical beams suffer from large fluctuations in their phase difference, which will degrade the sensitivity of the interferometer. We implement a phase lock loop using an EOM (labeled as 'EOM 1' in Fig. 1(a)) in the first arm to reduce such phase fluctuations. The output of the photodiode that contains the beat signal of the two optical beams is amplified and mixed with a reference signal. The output of the mixer is then passed through a low pass filter, an amplifier, and an integrator respectively before feeding it to the EOM to account for the error in the differential phase. We use two auxiliary outputs of the DDS (extracted from the main outputs of the DDS using RF power splitters) to generate the reference signal. Such outputs are filtered using appropriate band-pass filters and then doubled to account for the frequency doubling effect in SHGs. The outputs of the multipliers are again cleaned using a proper low-pass filter and then fed to an RF mixer. The output of the mixer is further amplified to produce the reference signal for the differential phase locking circuit.

3. Characterisation and results

We use the experimental setup described in [9] to evaluate the performance of our laser system. First, we prepare two laser-cooled ^{87}Rb clouds in $|F = 2\rangle$ atomic ground state at a temperature of $\approx 1.8\ \mu$K. We apply a light pulse resonant to $|F = 1\rangle \longrightarrow |F' = 1\rangle$ transition to depump the residual atoms left in $|F = 1\rangle$ ground state. Then, the Raman or Bragg processes are implemented and the atoms are finally detected at the bottom of the experiment using a state selective time of flight detection performed with horizontal sheets of light. The optical layout used to realize the Raman spectroscopy is shown in Fig. 1. The optical output of the laser system is fed to a collimator which produces a Gaussian beam of waist ≈ 6 mm. The output of the laser system contains two mutually perpendicular linearly polarized optical lasers. Such an output gets

Optics EXPRESS

transformed into $\sigma^+ - \sigma^-$ configuration after passing through the first quarter waveplate. After passing through a second quarter waveplate placed at the top, one of these two lasers is trashed from the upper PBS, whereas the other optical beam gets retro-reflected by the top mirror in the setup. Our schematic for the realization of the Raman spectroscopy using the sideband generation, technically differs from the conventional practice [21]. Rather than using a single phase-modulated laser beam, we use only the sidebands of one laser beam in conjugation with an unmodulated laser beam. In our laser system, [Fig. 1(a)], 'EOM 2' is placed in one of the paths to generate sidebands of the laser in that path. We drive this EOM to produce a maximum amount of power in the ±1 order sidebands at 780 nm. The frequency of the driving signal is chosen to be ≈ 6.834 GHz to address the two ground states of the ^{87}Rb atom. The common practice of realizing Raman transition using a single phase-modulated laser beam suffers from a modulation of the transition probability as a function of the distance of the atomic cloud from the top mirror [35]. A possible solution is to suppress one of the 1st order sidebands [36,37]. However, to overcome this problem, we choose to perform the Raman coupling using both the optical outputs from the two arms of our laser schematic. The optical layout of our system can be chosen such that the top mirror reflects back only the laser beam generated from 'Arm 1' due to its polarization state. Whereas, the other output generated from 'Arm 2' is reflected out of the setup from the top PBS. This leads to the possibility of having a Raman coupling with the laser beam coming out of 'Arm 2' and one of the sidebands of the laser beam out of 'Arm 1' and having identical circular polarization. By adding a proper offset (which we compensate again by shifting the freq difference between the two beams) to the micro-wave frequency fed to the 'EOM 2', one can meet the resonance condition with only one sideband from 'Arm 2' and the laser output from 'Arm 1'. Thus the coupling due to all other pairs of Raman beams can be neglected. Such a scheme provides the freedom of implementing the Raman process with optimal coupling efficiency at any distance between the atoms and the mirror. The PBS at the top, also suppresses the parasitic lattice that moves in the opposite direction and reduces the efficiency when realizing Bragg/Bloch process. However, a drawback for the use of this PBS is a potential degradation of the laser wavefront, which we have not characterized here. However, this effect shall be efficiently reduced in the differential gradiometric measurement.

We could also implement a double diffraction Raman spectroscopy [33] by removing the top PBS from the optical layout. Following the protocol given in Ref. [38], we apply a frequency to the 'EOM 2' to incorporate the lightshift along with the energy difference between the hyperfine ground states of ^{87}Rb. Simultaneously, the AOMs are driven with the frequency shift equal to the sum of the doppler detuning and recoil shift of the atoms to meet the resonance condition for both directions of the two-photon wavevector $\vec{\mathbf{k}}_\uparrow$ and $\vec{\mathbf{k}}_\downarrow$ wavevector.

In this section, we discuss the intensity noise and the remaining residual differential phase noise of the laser system. We found power instabilities of about 0.8% rms (1.5 mW over 187 mW) for Arm 1 and 0.6% rms (0.89 mW over 142 mW) for Arm 2 over 2.5 hour long monitorings of each of these powers. This measurement was performed at the output of the fiber, so as to be representative of the intensity fluctuations at the atoms. The Allan standard deviation of the power fluctuation is found to be 0.17 mW (ARM 1) and 0.14 mW (ARM 2) respectively in 1 s. In order to study the performance of the phase-lock in reducing the differential phase noise, we measure the phase noise with an FFT analyzer. The phase-lock electronics provides a buffered output to directly monitor the signal after the analog mixer. The blue curve in Fig. 2 displays the resulting amplitude spectral density of the phase error signal measured by feeding the buffered output of the mixer to the FFT analyzer in the closed loop condition while operating the phase-lock integrator at a gain for which the bandwidth of the lock is ∼ 10 kHz. In the absence of the phase lock, the phase fluctuations are too large (of more than a radian over a second) to make the FFT phase noise measurement as usual (keeping the phase close to mid fringe and with a linear (K_d) ratio between phase and voltage). As an alternative to performing a slow lock, we

Optics EXPRESS

rather measure the voltage corrections sent to the EOM 1 when the loop is closed. This provides, in the bandwidth of the lock, the phase fluctuations the lock compensates for. There, the linearity of the EOM and its sensitivity allows to track phase fluctuations over +- 10 rad and record an FFT spectrum (red curve in Fig. 2) of these fluctuations. Following the numerical recipe given in Ref. [39], we use the noise spectrum of our phase-lock and further estimate the residual phase noise in the case of a 2-pulse Ramsey and 3-pulse Mach-Zehnder interferometer. For a Ramsey interferometer, the remnant phase noise is found to be 1.7 mrad/shot for our experimental parameters ($T_R = 120$ ms, T_R being the total duration of the Ramsey interferometer). Whereas, for the 3-pulse Mach-Zehnder interferometer with similar experimental conditions ($2T_{MZ} = 240$ ms), the remnant phase noise from the differential phase fluctuation of the laser is found to be 2.6 mrad/shot.

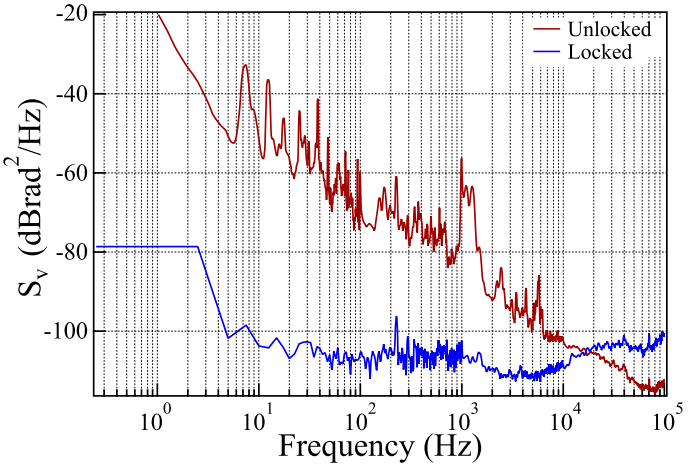

Fig. 2. Power spectral density of the lasers' differential phase fluctuations, for the phase-locked loop with bandwidth of about 10 kHz. 'Blue' and 'Red' curves represent measurement with and without the implementation of the lock respectively.

In order to experimentally demonstrate the effect of the phase-lock loop on the atoms, we set up a Ramsey interferometer ($T_R = 120$ ms) with two $\pi/2$ Raman pulses having a copropagating geometry. Such a clock-type interferometer is indeed not sensitive to vibration noise which typically largely exceeds the laser phase noise for long interferometer durations of the order of hundreds of ms, even with careful vibration isolation methods [40]. Hence such an interferometer scheme allows studying the effect of the residual laser phase noise on the atom interferometer. Figure 3 displays the modulation of the transition probability of both the atomic clouds of the gradiometer as a function of Raman detuning with and without the phase lock, respectively as 'solid' and 'dashed' traces. In the absence of the phase-lock, the Allan deviation of the phase fluctuations in each of the interferometer is found to be (180 ± 4) mrad/shot and (193 ± 4) mrad/shot. Whereas, after implementation of the phase lock this noise reduces to (14.7 ± 0.4) mrad/shot and (14.0 ± 0.4) mrad/shot respectively. Such a remnant noise is higher than calculated, but other sources of noise also contribute to this. For comparison, we also realized a similar Ramsey interferometer with microwave pulses instead of Raman lasers. We found interferometer phase noise of similar amplitudes (13.5 ± 0.3) mrad/shot and (14.6 ± 0.4) mrad/shot for the two atomic clouds respectively, which shows that our Raman Ramsey interferometer is limited in these measurements by the phase noise of the microwave reference and detection noise, more than by phase noise of the Raman lasers. This is consistent with the above calculation of the expected interferometer noise for a Ramsey interferometer using the phase spectral density (PSD)

Optics EXPRESS

and the transfer function of the interferometer, which amounts to a smaller contribution of ≈ 2 mrad/shot.

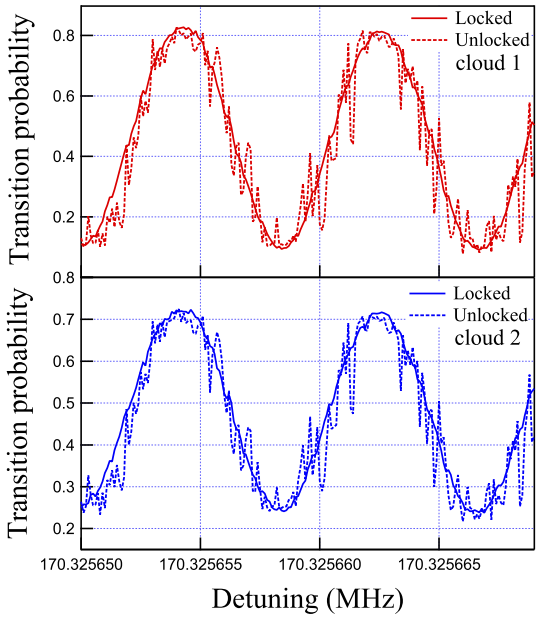

Fig. 3. Variation of transition probability of the atomic clouds (top and bottom panel) at the output of a Ramsey interferometer realized using two $\pi/2$ Raman pulses in copropagating configuration ($T_R = 120$ ms). The 'X'- axis records the detuning with respect to the hyperfine frequency between the two ground states of ^{87}Rb. The 'dashed' curves represent the effect of the phase noise introduced by the laser system in the absence of the phase-lock. The 'solid' curves show the reduction of the phase noise after the implementation of the phase lock.

Finally, we present in Fig. 4, the performance of the laser system by implementing a Bragg interferometer. Following the initial stage of state preparation as explained before, atoms are velocity selected using a Raman pulse with a long duration (100 μs). After this process, we apply a light resonant to $|F = 2\rangle \longrightarrow |F' = 3\rangle$ state to push away the atoms with higher velocity and left in $|F = 2\rangle$ state. Thus we are left with two velocity selected atomic clouds in $|F = 1\rangle$ state. We then realize a Bragg interferometer in a typical $\pi/2 - \pi - \pi/2$ Mach-Zehnder geometry. We could achieve a maximum efficiency of ~ 80% for a Bragg diffraction into $2\hbar$k state with a gaussian pulse of characteristic length (σ) 14 μs . The efficiency of the diffraction is limited by the output power of the laser system and the velocity width of the atomic cloud. The left panel in Fig. 4 shows a typical fringe pattern, obtained by measuring the transition probabilities for both the clouds as a function of frequency chirp applied to the frequency difference between the Bragg beams during the interferometer of $2T_{MZ} = 2$ ms. Finally, the right panel of Fig. 4 shows the ellipses corresponding to the correlated fluctuations of the transition probabilities as we increase the area of the interferometer by choosing $2T_{MZ} = 260$ ms. The differential sensitivity of the interferometer is found to be ~ 350 Eötvös/shot. This sensitivity is one order of magnitude above the best sensitivity (~ 30 E/$\sqrt{Hz}$ in [41] for a gravity gradiometer based on two-photon transition beamsplitters). Upgrades to our setup are underway in order to optimize the gradiometric sensitivity, thanks to the increase of the Bragg lasers beam size allowing for larger interferometer interrogation duration, to the improvement of the cooling laser system for

Optics EXPRESS

a larger number of cold atoms, and the installation of a tip-tilt mirror for Coriolis acceleration compensation [42].

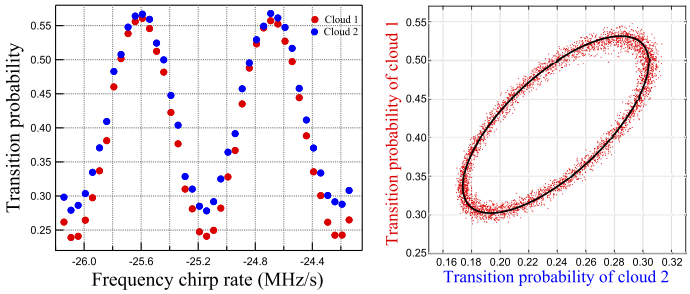

Fig. 4. Left panel: modulation of the transition probability for the two atomic clouds at the output of the Bragg interferometer with $2T_{MZ} = 2$ ms. Right Panel: Correlation between the transition probabilities of the two atomic clouds of the gradiometer at the output of a Bragg interferometer with $2T_{MZ} = 260$ ms.

4. Conclusion

In conclusion, we have demonstrated a simple, compact, and robust laser architecture that is capable of implementing a gradiometer in Raman or Bragg geometry. The architecture is mainly based on fiber-coupled optical elements which helps in alleviating misalignement issues, and thus offers excellent power stabilities of less than 1% rms. Also, the choice in the position of the optical elements in conjugation with the laser provides freedom to access over a large frequency range without sacrificing the output power of the system. It allows performing atom interferometers with different beamsplitter methods, with differential phase stabilities between beamsplitting lasers ~ 3 mrad/shot. In particular, we demonstrate preliminary measurements in a gradiometer configuration, whose sensitivity of 350 E/$\sqrt{Hz}$ still needs be improved to reach state of the art performance. The laser system will allow in the future to implement large momentum transfer with high order Bragg diffraction, and could be avantageously modified or complemented to allow for light shift compensation [43].

Funding. Direction Générale de l'Armement; Agence Nationale de la Recherche (ANR- 19-CE47-0003 GRADUS); Centre National de la Recherche Scientifique (PN-GRAM); Centre National d'Etudes Spatiales (R-S15/SU-0001-048, R-S19/SU-0001-048).

Acknowledgements. The authors thank Mehdi Langlois and Romain Caldani for their early contributions. R.P. thanks CNES and DGA for financial support.

Disclosures. The authors declare no conflicts of interest

Data Availability. Data underlying the results presented in this paper are not publicly available at this time but may be obtained from the authors upon reasonable request.

References

1. R. Geiger, A. Landragin, S. Merlet, and F. Pereira Dos Santos, "High-accuracy inertial measurements with cold-atom sensors," AVS Quantum Sci. **2**(2), 024702 (2020).
2. A. Peters, K. Y. Chung, and S. Chu, "Measurement of gravitational acceleration by dropping atoms," Nature **400**(6747), 849–852 (1999).
3. S. Merlet, Q. Bodart, N. Malossi, A. Landragin, F. P. D. Santos, O. Gitlein, and L. Timmen, "Comparison between two mobile absolute gravimeters: optical versus atomic interferometers," Metrologia **47**(4), L9–L11 (2010).
4. Z.-K. Hu, B.-L. Sun, X.-C. Duan, M.-K. Zhou, L.-L. Chen, S. Zhan, Q.-Z. Zhang, and J. Luo, "Demonstration of an ultrahigh-sensitivity atom-interferometry absolute gravimeter," Phys. Rev. A **88**(4), 043610 (2013).
5. C. Freier, M. Hauth, V. Schkolnik, B. Leykauf, M. Schilling, H. Wziontek, H.-G. Scherneck, J. Müller, and A. Peters, "Mobile quantum gravity sensor with unprecedented stability," J. Phys.: Conf. Ser. **723**, 012050 (2016).

Optics EXPRESS

6. V. Ménoret, P. Vermeulen, N. Le Moigne, S. Bonvalot, P. Bouyer, A. Landragin, and B. Desruelle, "Gravity measurements below 10^{-9} g with a transportable absolute quantum gravimeter," Sci. Rep. **8**(1), 12300 (2018).
7. M. J. Snadden, J. M. McGuirk, P. Bouyer, K. G. Haritos, and M. A. Kasevich, "Measurement of the earth's gravity gradient with an atom interferometer-based gravity gradiometer," Phys. Rev. Lett. **81**(5), 971–974 (1998).
8. F. Sorrentino, Q. Bodart, L. Cacciapuoti, Y.-H. Lien, M. Prevedelli, G. Rosi, L. Salvi, and G. M. Tino, "Sensitivity limits of a raman atom interferometer as a gravity gradiometer," Phys. Rev. A **89**(2), 023607 (2014).
9. R. Caldani, K. X. Weng, S. Merlet, and F. Pereira Dos Santos, "Simultaneous accurate determination of both gravity and its vertical gradient," Phys. Rev. A **99**(3), 033601 (2019).
10. T. L. Gustavson, A. Landragin, and M. A. Kasevich, "Rotation sensing with a dual atom-interferometer sagnac gyroscope," Classical Quantum Gravity **17**(12), 2385–2398 (2000).
11. I. Dutta, D. Savoie, B. Fang, B. Venon, C. L. Garrido Alzar, R. Geiger, and A. Landragin, "Continuous cold-atom inertial sensor with 1 nrad/sec rotation stability," Phys. Rev. Lett. **116**(18), 183003 (2016).
12. J. B. Fixler, G. T. Foster, J. M. McGuirk, and M. A. Kasevich, "Atom interferometer measurement of the newtonian constant of gravity," Science **315**(5808), 74–77 (2007).
13. G. Rosi, F. Sorrentino, L. Cacciapuoti, M. Prevedelli, and G. M. Tino, "Precision measurement of the newtonian gravitational constant using cold atoms," Nature **510**(7506), 518–521 (2014).
14. D. DiFrancesco, A. Grierson, D. Kaputa, and T. Meyer, "Gravity gradiometer systems – advances and challenges," Geophys. Prospect. **57**(4), 615–623 (2009).
15. S.-w. Chiow, T. Kovachy, H.-C. Chien, and M. A. Kasevich, "102$\hbar k$ large area atom interferometers," Phys. Rev. Lett. **107**(13), 130403 (2011).
16. H. Müller, S. wey Chiow, Q. Long, and S. Chu, "Phase-locked, low-noise, frequency agile titanium:sapphire lasers for simultaneous atom interferometers," Opt. Lett. **31**(2), 202–204 (2006).
17. S. Chiow, T. Kovachy, J. M. Hogan, and M. A. Kasevich, "Generation of 43 w of quasi-continuous 780 nm laser light via high-efficiency, single-pass frequency doubling in periodically poled lithium niobate crystals," Opt. Lett. **37**(18), 3861–3863 (2012).
18. S. S. Sané, S. Bennetts, J. E. Debs, C. C. N. Kuhn, G. D. McDonald, P. A. Altin, J. D. Close, and N. P. Robins, "11 w narrow linewidth laser source at 780nm for laser cooling and manipulation of rubidium," Opt. Express **20**(8), 8915–8919 (2012).
19. M. Kim, R. Notermans, C. Overstreet, J. Curti, P. Asenbaum, and M. A. Kasevich, "40 w 780 nm laser system with compensated dual beam splitters for atom interferometry," Opt. Lett. **45**(23), 6555–6558 (2020).
20. F. Lienhart, S. Boussen, O. Carraz, N. Zahzam, Y. Bidel, and A. Bresson, "Compact and robust laser system for rubidium laser cooling based on the frequency doubling of a fiber bench at 1560 nm," Appl. Phys. B **89**(2-3), 177–180 (2007).
21. O. Carraz, F. Lienhart, R. Charrière, M. Cadoret, N. Zahzam, Y. Bidel, and A. Bresson, "Compact and robust laser system for onboard atom interferometry," Appl. Phys. B **97**(2), 405–411 (2009).
22. M. Schmidt, M. Prevedelli, A. Giorgini, G. M. Tino, and A. Peters, "A portable laser system for high-precision atom interferometry experiments," Appl. Phys. B **102**(1), 11–18 (2011).
23. S. Merlet, L. Volodimer, M. Lours, and F. Pereira Dos Santos, "A simple laser system for atom interferometry," Appl. Phys. B **117**(2), 749–754 (2014).
24. Q. Wang, Z. Wang, Z. Fu, W. Liu, and Q. Lin, "A compact laser system for the cold atom gravimeter," Opt. Commun. **358**, 82–87 (2016).
25. V. Schkolnik, O. Hellmig, A. Wenzlawski, J. Grosse, A. Kohfeldt, K. Döringshoff, A. Wicht, P. Windpassinger, K. Sengstock, C. Braxmaier, M. Krutzik, and A. Peters, "A compact and robust diode laser system for atom interferometry on a sounding rocket," Appl. Phys. B **122**(8), 217 (2016).
26. X. Wu, F. Zi, J. Dudley, R. J. Bilotta, P. Canoza, and H. Müller, "Multiaxis atom interferometry with a single-diode laser and a pyramidal magneto-optical trap," Optica **4**(12), 1545–1551 (2017).
27. J. Fang, J. Hu, X. Chen, H. Zhu, L. Zhou, J. Zhong, J. Wang, and M. Zhan, "Realization of a compact one-seed laser system for atom interferometer-based gravimeters," Opt. Express **26**(2), 1586–1596 (2018).
28. Q. Luo, H. Zhang, K. Zhang, X.-C. Duan, Z.-K. Hu, L.-L. Chen, and M.-K. Zhou, "A compact laser system for a portable atom interferometry gravimeter," Rev. Sci. Instrum. **90**(4), 043104 (2019).
29. R. Caldani, S. Merlet, F. Pereira Dos Santos, G. Stern, A. Martin, B. Desruelle, and V. Ménoret, "A prototype industrial laser system for cold atom inertial sensing in space," Eur. Phys. J. D **73**(12), 248 (2019).
30. D. O. Sabulsky, J. Junca, G. Lefévre, X. Zou, A. Bertoldi, M. Battelier, B. andPrevedelli, G. Stern, J. Santoire, Q. Beaufils, R. Geiger, A. Landragin, B. Desruelle, P. Bouyer, and B. Canuel, "A fibered laser system for the miga large scale atom interferometer," Sci. Rep. **10**(1), 3268 (2020).
31. D. M. S. Johnson, J. M. Hogan, S. w. Chiow, and M. A. Kasevich, "Broadband optical serrodyne frequency shifting," Opt. Lett. **35**(5), 745–747 (2010).
32. R. J. Thompson, M. Tu, D. C. Aveline, N. Lundblad, and L. Maleki, "High power single frequency 780nm laser source generated from frequency doubling of a seeded fiber amplifier in a cascade of ppln crystals," Opt. Express **11**(14), 1709–1713 (2003).
33. T. Lévèque, A. Gauguet, F. Michaud, F. Pereira Dos Santos, and A. Landragin, "Enhancing the area of a raman atom interferometer using a versatile double-diffraction technique," Phys. Rev. Lett. **103**(8), 080405 (2009).

Optics EXPRESS

34. T. Lévèque, L. Antony Micollier, B. Faure, and J. Berthon, "A laser setup for rubidium cooling dedicated to space applications," Appl. Phys. B **116**(4), 997–1004 (2014).
35. O. Carraz, R. Charrière, M. Cadoret, N. Zahzam, Y. Bidel, and A. Bresson, "Phase shift in an atom interferometer induced by the additional laser lines of a raman laser generated by modulation," Phys. Rev. A **86**(3), 033605 (2012).
36. C. Rammeloo, L. Zhu, Y.-H. Lien, K. Bongs, and M. Holynski, "Performance of an optical single-sideband laser system for atom interferometry," J. Opt. Soc. Am. B **37**(5), 1485–1493 (2020).
37. S. Templier, J. Hauden, P. Cheiney, F. Napolitano, H. Porte, P. Bouyer, B. Barrett, and B. Battelier, "Carrier-suppressed multiple single-sideband laser source for atom cooling and interferometry," (2021).
38. N. Malossi, Q. Bodart, S. Merlet, T. Lévèque, A. Landragin, and F. P. D. Santos, "Double diffraction in an atomic gravimeter," Phys. Rev. A **81**(1), 013617 (2010).
39. P. Cheinet, B. Canuel, F. Pereira Dos Santos, A. Gauguet, F. Yver-Leduc, and A. Landragin, "Measurement of the sensitivity function in a time-domain atomic interferometer," IEEE Trans. Instrum. Meas. **57**(6), 1141–1148 (2008).
40. J. Le Gouët, T. Mehlstäubler, J. Kim, S. Merlet, A. Clairon, A. Landragin, and F. Pereira Dos Santos, "Limits to the sensitivity of a low noise compact atomic gravimeter," Appl. Phys. B **92**(2), 133–144 (2008).
41. J. M. McGuirk, G. T. Foster, J. B. Fixler, M. J. Snadden, and M. A. Kasevich, "Sensitive absolute-gravity gradiometry using atom interferometry," Phys. Rev. A **65**(3), 033608 (2002).
42. S.-Y. Lan, P.-C. Kuan, B. Estey, P. Haslinger, and H. Müller, "Influence of the coriolis force in atom interferometry," Phys. Rev. Lett. **108**(9), 090402 (2012).
43. T. Kovachy, P. Asenbaum, C. Overstreet, C. A. Donnelly, S. M. Dickerson, A. Sugarbaker, J. M. Hogan, and M. A. Kasevich, "Quantum superposition at the half-metre scale," Nature **528**(7583), 530–533 (2015).